Supplemental Mineralogical Methods Graphs Data

Table S1. Mineral (%) from XRD.

Sample	Quartz	Microcline	Kaolinite	Illite	Orthoclase	Labradorite	Calcite	Muscovite	Anorthite	Paragonite	Albite	Total	Rwp	S	Chi^2
Pottery 1	35.00%	15.00%	4.30%	13.00%	3.80%	6.00%	6.30%	14.40%	1.80%	0.00%	1.10%	100.70%	13.33%	1.2086	1.4607
Pottery 2	26.00%	1.20%	0.09%	4.40%	0.00%	0.41%	0.00%	37.00%	11.50%	0.00%	17.70%	98.30%	14.85%	1.5182	2.3048
Pottery 3	47.00%	1.40%	0.07%	0.60%	2.50%	16.40%	0.20%	10.30%	5.90%	1.10%	14.80%	100.27%	12.95%	1.3250	1.7556

Sample	Quartz	Microcline	Kaolinite	Illite	Orthoclase	Labradorite	Calcite	Muscovite	Anorthite	Paragonite	Albite	Total	Rwp	S	Chi^2
*Figurine	5.50%	7.00%	4.60%	1.60%	7.10%	34.60%	0.00%	1.60%	14.10%	0.00%	0.00%	100.00%	--	--	2.76

*Data provided by David Price (2018), University of Wollongong, Wollongong, Australia.

Figure S1. Mineral peaks from XRD. Pottery sample 1. Baked glacial clay sourced from Ross County, Ohio.

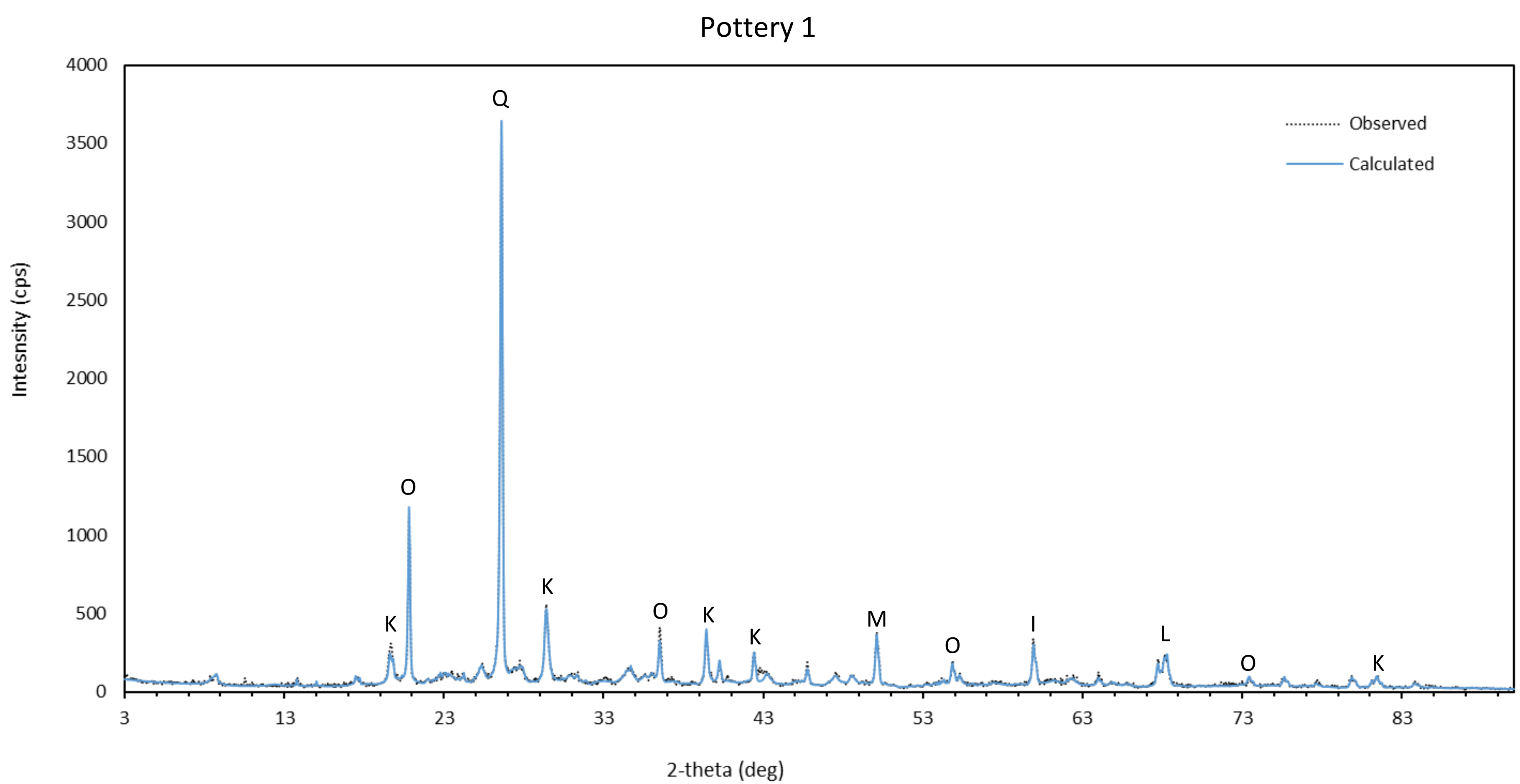

Mineral abbreviations: Pa = Paragonite; A = Albite; Q = Quartz; K = Kaolinite; I = Illite; M = Muscovite; O = Orthoclase; L = Labradorite.

Figure S2. Mineral peaks from XRD. Pottery sample 2. Grit tempered pottery sample (1 of 2) from the Cash Site, Ross County, Ohio.

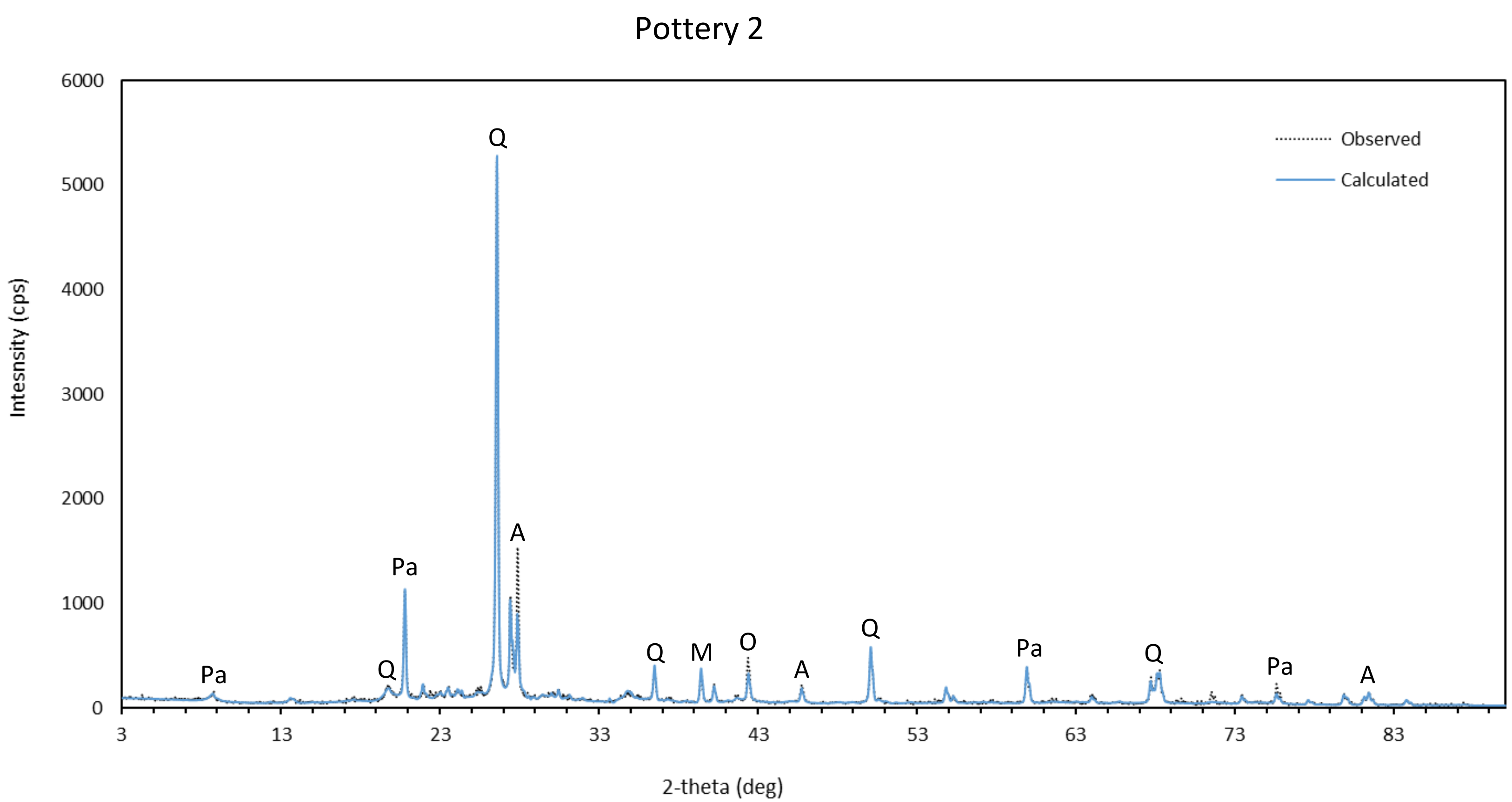

Figure S3. Mineral peaks from XRD. Pottery sample 3. Grit tempered pottery sample (2 of 2) from the Cash Site, Ross County, Ohio.

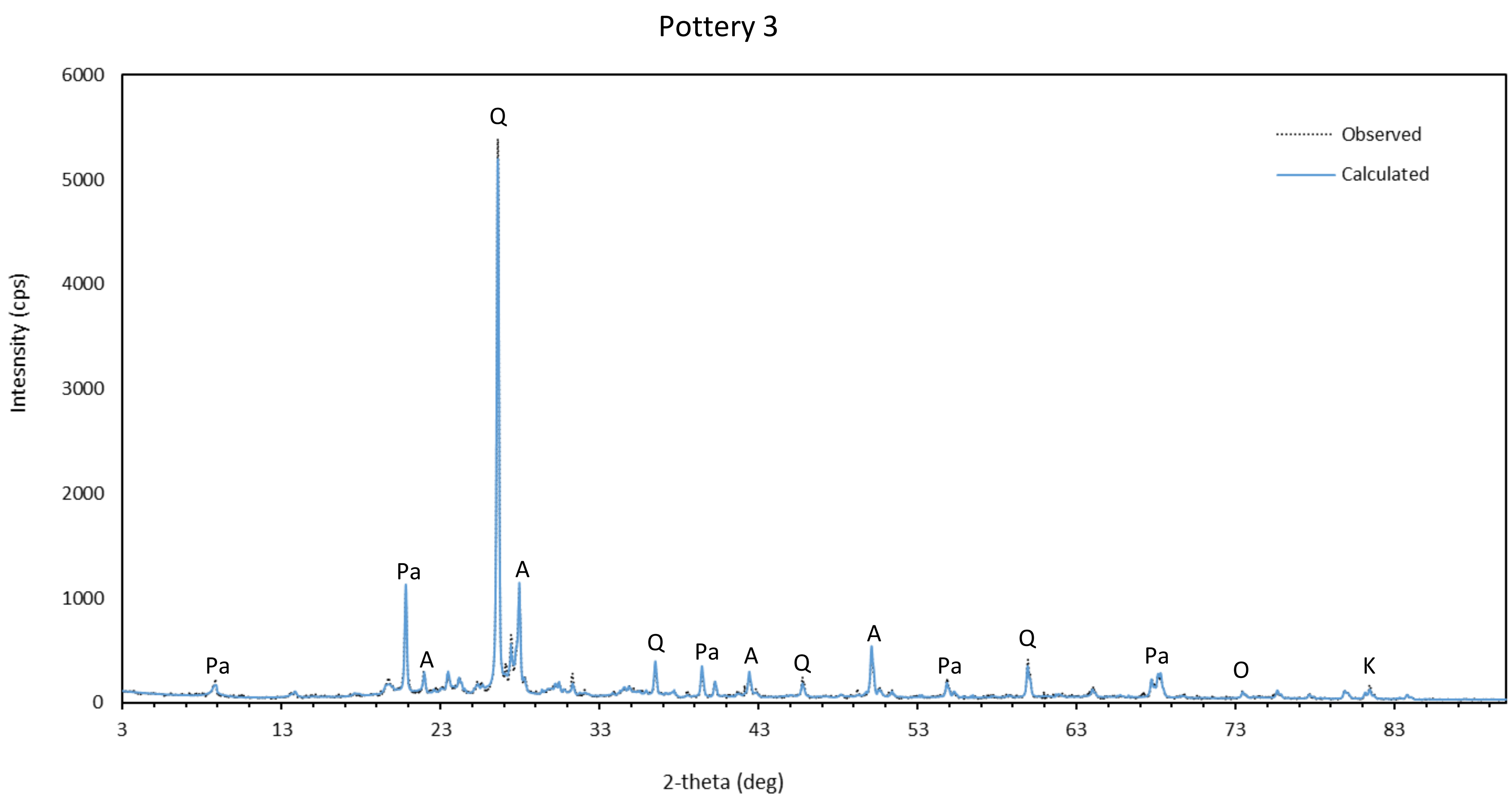

Figure S4. Mineral peaks from XRD from the figurine. The Al peak is due to the aluminum sample holder.

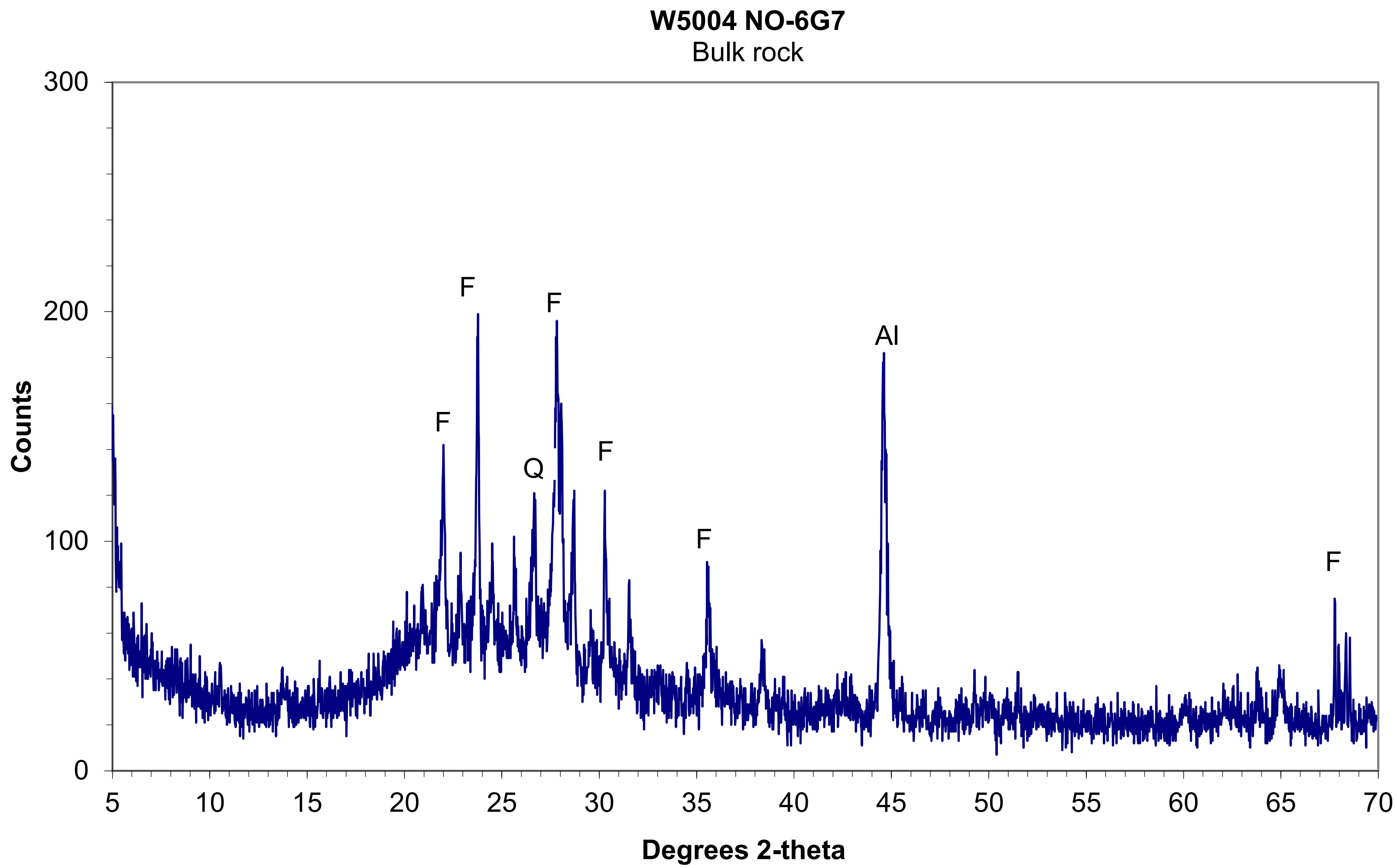

XRD Methods

Mineral composition of a milled subsample for each pottery sample was determined by powder X-ray diffraction using a MiniFlex 6G Benchtop X-Ray Diffractometer (Rigaku) with a D/teX Ultra2 detector operated with a Cu X-ray tube (λ = 1.5406 Å) at 40 kV and 15 mA. Counts were collected from 3° to 90° with a step size of 0.02° and a speed of 2.0° per minute. Phase identification and quantitative analysis of minerals were performed using Rigaku's PDXL software, utilizing the whole pattern powder fitting (WPPF) method, connected to the ICDD PDF-2 mineral database. To fit the peaks the split pseudo-Voigt function and the B-spline background model were used. The fitting quality of the experimental data was confirmed by using the goodness of fit term (S), which should be close to 1 for a good fit, and the reliability factor Rwp (weighted difference between measured and calculated profile values), which should be close to or less than 10%.

XRD Results

The figurine's major mineralogical components are primarily plagioclase and k-feldspar bearing minerals accounting for 83.8%; the figurine has more kaolinite (4.6%) than illite (1.6%). This mineralogical composition is much different from that of the three pottery samples, where the dominant minerals are quartz and clay-associated minerals, muscovite and illite, with lower kaolinite content and significantly smaller ratios of plagioclase and k-feldspar bearing minerals.

Major Element Composition

Methods

Pottery samples (Figure S5) were powdered using a marble mortar and pestle and SPEX Ball Mill. Loss on ignition (LOI) was performed on powdered pottery samples to remove any volatiles. Ash powdered pottery samples were mixed with lithium tetraborate flux and fused together to create a glass bead using a LeoNeo Flux Fusion system. Glass beads were measured on the Malvern Panalytical Epsilon 3XLE energy dispersive X-ray fluorescence spectrometer (EDXRF). We measured USGS standard Brush Creek Shale (SBC-1) to monitor EDXRF accuracy and precision. SBC-1 was within 5% error of certified USGS values, except for Na_2O, which was not measured.

Figure S5. Picture of pottery samples and ID.

Results

Table S2. Major Element Composition of Pottery Samples.

Sample ID	Na_2O (wt.%)	MgO (wt.%)	Al_2O_3 (wt.%)	SiO_2 (wt.%)	P_2O_5 (wt.%)	K_2O (wt.%)	CaO (wt.%)	TiO_2 (wt.%)	MnO (wt.%)	Fe_2O_3 (wt.%)	LOI (wt.%)	Total
Pottery 1	0.461	5.318	12.348	53.407	--	2.922	9.932	0.684	0.058	5.89	7.51	98.53
Pottery 2	1.022	0.528	15.658	64.844	1.225	2.415	1.466	0.654	0.014	4.092	7.75	99.668
Pottery 3	1.987	0.693	15.374	61.691	1.051	2.353	2.021	0.593	0.023	3.77	10.17	99.726
Figurine* (adjusted)	0.677	0.904	12.632	61.964	0.524	4.410	5.047	1.125	0.122	9.444	--	96.848
SBC-1	--	2.221	22.768	49.099	0.251	3.845	0.516	0.882	0.04	9.632	10.06	99.314

*Denotes a different form of measurement and calculation for the figurine. Due to the importance of the sample, we could not manipulate it to obtain LOI values or utilize the fusion method to analyze the figurine. These values are reflective of the proportion distribution of the raw data of a bulk measurement on the EDXRD and values normalized of the total raw major elemental concentration of 96.848 (wt. %).

The major elemental composition of pottery samples suggests clay content. Adopting the Fedo et alia (1995) strategy in understanding the parent source of siliciclastic material, we implemented this technique to understand the sources of the pottery and the figurine. The chemical composition of these artifacts derived from siliciclastic material; this material can be plotted as molar proportions within Al_2O_3, CaO* (CaO associated with silicates) + Na_2O, and K_2O (A-CN-K) compositional space, where CaO* represents Ca in silicate-bearing minerals only (Fedo et al. 1995). This makes the A-CN-K system useful for evaluating fresh rock compositions and examining their weathering trends due to the dominance of plagioclase-feldspar–rich and K-feldspar–rich rocks on the continental crust (Nesbitt and Young 1984, 1989). This includes weathering by-products like clay minerals, which were used to make pottery and prehistoric figurines. Utilizing the A-CN-K system, we observe differences in parental sources between the pottery samples and the figurine. The pottery derives from a more plagioclase source, whereas the figurine source has more K-feldspar. This supports our theory that the figurine is not from the same source as the pottery.

References Cited

Fedo, Christopher M., H. Wayne Nesbitt, and Grant M. Young (1995) Unraveling the Effects of Potassium Metasomatism in Sedimentary Rocks and Paleosols, With Implications for Paleoweathering Conditions and Provenance. *Geology* 23:921–924. https://doi.org/10.1130/0091-7613(1995)023<0921:UTEOPM>2.3.CO;2, accessed September 13, 2021.

Nesbitt, H. Wayne, and Grant M. Young (1984) Prediction of Some Weathering Trends of Plutonic and Volcanic Rocks Based on Thermodynamic and Kinetic Considerations. *Geochimica et Cosmochimica Acta* 48:1523–1534. https://doi.org/10.1016/0016-7037(84)90408-3, accessed September 13, 2021.

Nesbitt, H. Wayne, and Grant M. Young (1989) Formation and Diagenesis of Weathering Profiles. *Journal of Geology* 97:129–147. http://dx.doi.org/10.1086/629290, accessed September 13, 2021.